

# On-Demand Millisecond Storage of Spectro-Temporal Multimode Telecom Photons

Anuj Sethia ,<sup>1,2</sup> Nasser Gohari Kamel ,<sup>1,2</sup> and Daniel Oblak ,<sup>1,2,\*</sup>

<sup>1</sup>*Department of Physics and Astronomy, University of Calgary, Calgary, AB T2N 1N4, Canada.*

<sup>2</sup>*Institute of Quantum Science and Technology, University of Calgary, Calgary, AB T2N 1N4, Canada.*

(Dated: December 22, 2025)

The realization of scalable quantum networks for distribution of entanglement over long distances hinges on quantum repeaters. To outperform the exponential transmission loss in optical fibers, quantum repeaters must employ multiplexing schemes in the temporal, spectral, or spatial domain. The performance of such a multiplexed scheme is contingent on efficient quantum memories offering both extended storage times and large multimode capacities. In this work, we experimentally demonstrate such a memory operating at telecom wavelength using an  $\text{Er}^{3+};\text{Y}_2\text{SiO}_5$  crystal. Using single-photon detectors, we record on-demand storage and recall of weak coherent pulses for up to 1 ms, exceeding that of previously reported quantum memories based on  $\text{Er}^{3+}$ . The memory exhibits an efficiency of 10.36% at 300  $\mu\text{s}$  storage time with a signal-to-noise ratio of 10.9. We further showcase its multimode capacity by storing 20 temporal and 3 spectral modes simultaneously with on-demand and selective recall capabilities, essential for a scalable quantum repeater architecture.

Future quantum networks [1, 2] are envisioned to enable transformative applications, such as distributed quantum computing [3, 4], quantum-enhanced distributed sensing [5–7], precise clock distribution [8], and secure communication [9]. Since exponential photon loss in optical fibers limits the communication link distances, quantum repeaters (QRs) [10, 11] are essential to implement such long-range quantum networks. To achieve practical entanglement distribution rates, most QR protocols require high-performance quantum memories (QMs) [12–14]. Specifically, QMs must offer a wide bandwidth, high multimode capacity, high storage efficiency, and storage times on the order of milliseconds, equivalent to the round trip time over the link [14, 15]. The development of such high-performance QMs requires both the exploration of new material platforms and the advancement of implementation protocols.

Rare-earth ion-doped crystals are a leading candidate for QMs due to their long coherence lifetimes [16–18], along with their proven multimode capacity [19–23], wide bandwidths [14, 15], and potential for near-unity storage efficiency [24, 25]. Among these, erbium ions ( $\text{Er}^{3+}$ ) are particularly compelling because their optical transition falls within the telecom C-band. This critical property enables  $\text{Er}^{3+}$ -based QM to interface directly with existing low-loss telecommunication fiber infrastructure, positioning them as an ideal platform for scalable, long-distance quantum networks. Such QMs have been successfully demonstrated across a range of host platforms, including optical fibers [22, 26–29],  $\text{LiNbO}_3$  [30, 31], and  $\text{Y}_2\text{SiO}_5$  [32–36], with additional promising platforms continuously being explored [37, 38]. Although host platforms such as  $\text{Y}_2\text{SiO}_5$  exhibit coherence times up to 4 ms [39, 40], the longest storage time demonstrated to date is only 110  $\mu\text{s}$  [41]. Achieving practical millisecond-scale storage along with multimode capacity, as required for QRs, therefore, remains an open challenge.

An important challenge limiting longer storage times

arises from the QM protocol itself. The Atomic Frequency Comb (AFC)-based [19] schemes face inherent constraints due to the difficulty of preparing sufficiently narrow comb structures [42, 43]. Furthermore, spin-wave storage—which would enable both extended storage times and on-demand recall—has not yet been demonstrated in  $\text{Er}^{3+}$ -based systems, due to the complexity of resolving the spin transitions within the inhomogeneous linewidth [44–47]. The Revival of Silenced Echo (ROSE) protocol [48–50] offers long storage time and on-demand recall capabilities; however, its reliance on spatial mismatch of optical fields makes it difficult to implement on a scalable integrated platform.

In this work, we present the Chirped Pulse Phase Encoding (CPPE) protocol [51, 52] in the context of its application to spectro-temporally multiplexed QR architectures aimed at long-distance quantum networks. We first identify the performance requirements a QM must meet to enhance entanglement distribution in a QR compared to direct fiber transmission. Furthermore, we experimentally demonstrate on-demand storage of telecom photons using  $\text{Er}^{3+}$  ions doped in  $\text{Y}_2\text{SiO}_5$  using the CPPE protocol. We achieve storage of weak coherent pulses for durations ranging from 300  $\mu\text{s}$  up to 1 ms, with efficiency of 10.36% and 1.42%, respectively. Additionally, we realize a multimode capacity comprising 20 temporal and 3 spectral modes at a storage time of 800  $\mu\text{s}$ , representing a significant step toward practical QR implementations.

*Multiplexed Quantum Repeater*—The overall entanglement distribution rate over the elementary links of a QR is constrained by the probabilistic nature of entangled-pair generation and fiber transmission, non-unit detector efficiencies, the inherent limitations of Bell-state measurements (BSM) with linear optics, and finite QM efficiency. Fortunately, these limitations can be overcome by multiplexing a large number of modes in various degrees of freedom, such as time, frequency, or space [20, 21, 23, 54]. By attempting entanglement distri-

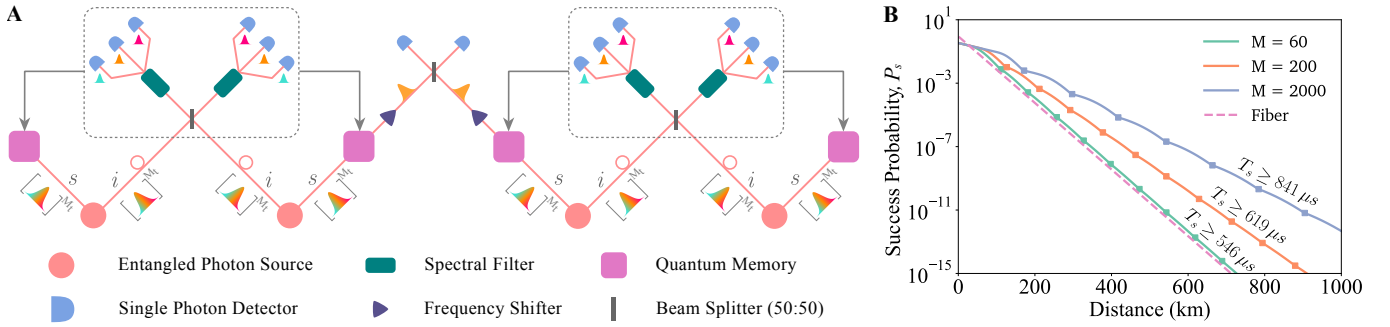


FIG. 1. (A) Illustration of a spectro-temporal multiplexed quantum repeater with two elementary links. The protocol begins with the generation of  $M_t$  entangled photon pairs simultaneously across  $M_s = 3$  spectral modes using probabilistic non-linear sources. The signal photons ( $s$ ) are stored in an on-demand QM, while the idler photons ( $i$ ) travel through the channel for entanglement swapping. Idler photons from adjacent nodes interfere on a 50:50 beam splitter and are spectrally resolved for individual detection. A successful BSM triggers a feedback signal to recall the corresponding spectral mode from the QM, followed by an appropriate frequency shift for the subsequent swapping between signal photons of neighboring links. (B) Entanglement distribution success probability  $P_s$  as a function of distance. The solid curves show the performance of a quantum repeater for different total multimode capacity  $M = M_t \times M_s$  given memory parameters  $\eta_o = 65\%$  and  $T_2 = 3$  ms. The pink dashed curve represents direct transmission through SMF-28 fiber. The success probability is optimized for the number of elementary links ( $n_l$ ), and the squares represent an increment in  $n_l$  starting from  $n_l = 1$ . Additionally, the minimum QM storage time ( $T_s$ ) required for each scenario is estimated. See Supplemental Material [53] for details on simulation parameters.

bution across many modes in parallel, the overall success probability of entanglement swapping over all the elementary links can approach unity. However, implementing such a scheme requires a multimode QM capable of storing as well as selectively retrieving a large number of modes.

If provided with a QM featuring both spectral and temporal multimode capacity, one may incorporate it in the multiplexed QR scheme illustrated in Fig. 1A. The focus on spectral multiplexing, in addition to temporal multiplexing, is due to its compatibility with common broadband entangled photon pair sources, e.g., those based on spontaneous parametric down-conversion (SPDC). A key challenge in typical spectral multiplexing schemes is, however, the need for resolving the different spectral modes before detection at each node [20]. Our QR architecture overcomes this obstacle significantly by leveraging the QM's inherent selective recall capabilities, thus substantially reducing the architecture complexity.

QMs with high multimode capacities have been demonstrated [22, 42], but have been limited by short, fixed storage times and low retrieval efficiencies, which restrict their usefulness in long-distance quantum networks. To systematically identify the memory specifications required for a QR to surpass direct transmission using the same photon-pair source, we develop an elementary model of the entanglement distribution success probability  $P_s$  as a function of distance (see [53] for analytic expression). The storage efficiency of our memory is suitably fitted by an exponential decay as  $\eta_M^s(T_s) = \eta_o \exp[-4T_s/T_2]$ , where  $\eta_o$  is the memory efficiency in the limit of zero storage time and  $T_2$  the memory coherence time. On the other hand, the roundtrip travel of

signals between the memory and the BSM over an elementary link prescribes the required storage time in a QR as  $T_s = L/(n_l v)$ , where  $L$  the total link distance,  $n_l$  the optimal number of elementary links, and  $v$  the speed of light in glass. Based on these dependencies, the success probability  $P_s$  is plotted for different memory parameters in Fig. 1B, along with the success probability for direct transmission. Of course, direct transmission may feature less limitations to pulse-bandwidths and, thus, realistically allow higher repetition rates  $\nu$ . In this case, more stringent requirements for memory performance must be met, for the overall entanglement distribution rate  $\nu \times P_s$  to exceed that for direct transmission.

The plot highlights the performance threshold a QM must meet to provide a genuine advantage. For instance, when the optimal repeater configuration yields elementary links of 200 km, then storage times,  $T_s$ , on the order of 1 ms are required to bridge classical-communication delays. This in turn, requires the QM platform to feature a storage efficiency of at least  $\eta_o \geq 65\%$ , a coherence time of  $T_2 \geq 3$  ms, and support a multimode capacity of  $M \geq 60$  modes. More details of the model and assumptions are provided in the Supplemental Material [53]. Our QM platform addresses the simultaneous requirements of multimode capacity, high efficiency, and millisecond-scale storage times, and provides a clear path toward achieving the performance needed for practical repeater operation.

*Experiment*— As a memory platform, we utilize a 5 ppm  $^{167}\text{Er}^{3+}:\text{Y}_2\text{SiO}_5$  crystal due to its long coherence properties [40, 55]. We are specifically focusing on the crystallographic site 1 (1536.4 nm) class of ions due to the higher optical depth of about 2, which maximizes storage efficiency (see supplementary material [53] for

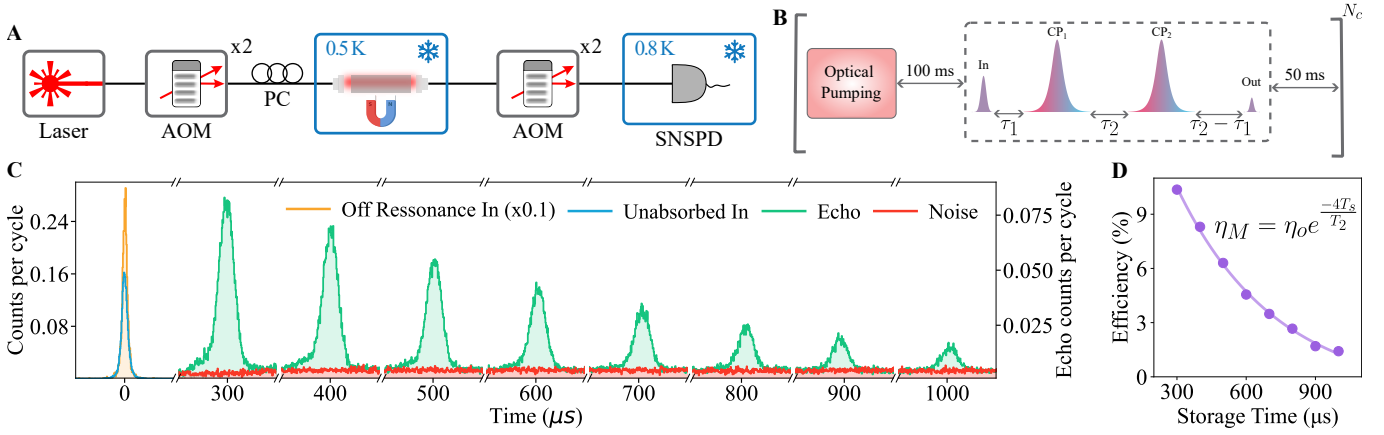


FIG. 2. (A) Schematic of the experimental setup. The two Acousto-Optic Modulators (AOMs) before the crystal prepare input modes and the chirp pulses (CP). The AOMs after the crystal, with combined efficiency of  $\eta_{\text{AOM}} = 35\%$ , allow only the input and desired echo to pass through for detection via Superconducting Nanowire Single Photon Detector (SNSPD), featuring  $\eta_{\text{D}} = 67\%$  detection efficiency. (B) Illustration of the pulse sequence for a storage cycle of the CPPE memory protocol. The storage and recall of input modes is performed using CP<sub>1</sub> and CP<sub>2</sub>, as shown in the dashed box. (C) Timing histogram of photon counts from SNSPD for  $N_c = 9000$  cycles. The leftmost panel showcases the off-resonance input, with an estimated mean photon number of 720 before the crystal, and the unabsorbed input during the memory sequence. Other panels display the recalled echo and the noise (measured without the input) for experiments with different storage times. The SNR of the recalled echo is 10.90 for 300  $\mu\text{s}$  and 1.52 for 1 ms. (D) The experimental memory retrieval efficiency is plotted against storage time and fitted with an exponential decay [23]. The fit's decay constant yields the coherence time,  $T_2 = 858.4 \pm 80.4 \mu\text{s}$  and  $\eta_o = 23.05\%$ .

absorption profile). The crystal is housed in a continuously pumped He-3 cryostat, maintained at a temperature of approximately 500 mK. The light is coupled into the crystal using single-mode fibers with pigtailed ferrules and Gradient Index (GRIN) lenses at both ends of the crystal. The components are self-aligned using a V-groove assembly, resulting in a total optical transmission of approximately  $\eta_T = 20\%$ . This compact and simple setup eliminates the need for costly nano-positioners or complex free-space setups, thus, simplifying the implementation for large-scale quantum networks. A vector magnet applies a static magnetic field of 3 T oriented at an angle of 135° relative to the  $D_1$  axis along the  $D_1 - D_2$  plane of the crystal. We measure optical coherence time,  $T_2 = 806.1 \pm 38.3 \mu\text{s}$ , using the two-pulse photo echo technique [53].

In our experimental setup, as depicted in Fig. 2A, an external cavity diode laser and two Acousto-Optic Modulators (AOMs) are used to set the laser frequency to the peak absorption of the site 1 transition at 1536.056 nm under the applied magnetic field. The AOMs generate both the weak coherent input probe-pulses and the strong chirped pulses needed for the CPPE protocol. After transmission from the crystal, two additional AOMs suppress all light except the input and echo signals, preventing saturation of the Superconducting Nano-Wire Single-Photon Detector (SNSPD) by the chirped control-pulses. The AOMs also serve as frequency shifters to match the frequency of retrieved spectral modes in the described QR scheme in Fig. 1A.

To ensure consistent performance, each storage cycle begins with a 50 ms optical pumping step. This process resets the atomic population from the previous cycle, thereby avoiding a decrease in storage efficiency. The pumping transfers population from the surrounding region into the memory region, creating spectral pits approximately 5 MHz wide on either side of the memory window. Following this, we include a 100 ms wait time to allow for the spontaneous decay of ions back to the ground state manifold, as the optical lifetime is measured to be about 10 ms [53]. The CPPE memory protocol sequence, depicted in Fig. 2B, begins with the input pulses to be stored at  $t = 0$ . After a delay of  $\tau_1$ , a chirped pulse (CP) with a duration of  $\tau_{\text{CP}}$  is applied to adiabatically flip the population of the atomic ensemble. The CP pulse,  $P(t) = A(t) \sin(\phi(t))$ , has sech hyperbolic envelope combined with a linear frequency sweep:

$$A(t) = A_0 \operatorname{sech} \left( \frac{10t}{\tau_{\text{CP}}} \right), \quad \frac{d\phi}{dt} = \omega(t) = \omega_0 + \frac{2t\Delta}{\tau_{\text{CP}}}. \quad (1)$$

The adiabatic chirp of this pulse imprints a detuning-dependent phase onto the atoms, which suppresses the primary echo [51, 52]. Moreover, the adiabatic nature of the population transfer makes CPPE robust to power and frequency fluctuations [52]. The span of the frequency chirp ( $\Delta$ ) is optimized to cover the entire spectrum of the input pulse while avoiding the excitation of any additional ions, thereby reducing noise from spontaneous emission [56, 57]. To retrieve the stored input modes, an identical second CP is applied after a delay of  $\tau_2$ . The

atomic ensemble subsequently re-emits the echo of the input mode after a duration of  $\tau_2 - \tau_1$ , resulting in a total storage time of  $T_s = 2(\tau_2 + \tau_{CP})$ .

Although the protocol is designed to suppress the primary probe-echo, imperfections in the CP can result in an “unsilenced” echo being present. To prevent this unwanted echo from overlapping with the desired output, we set the timing of CP such that  $2\tau_1 < \tau_2$ . Additionally, the protocol also results in an echo from the CPs themselves occurring after the recall of input modes, which is suppressed by a second pair of AOMs.

The weak coherent probe-pulses are prepared as a Lorentzian shaped with a full-width at half-maximum (FWHM) of  $0.75\ \mu\text{s}$ . We demonstrate on-demand storage of weak coherent probe-pulses for various storage times ranging from  $300\ \mu\text{s}$  to  $1\ \text{ms}$ , as shown in Fig. 2C. The estimated mean photon number of the input probe-pulse  $n_{\text{in}}$  is approximately 720 before the crystal with  $\eta_T = 20\%$  transmission to the output fiber off atomic resonance. As depicted in Fig. 2D, the storage efficiency  $\eta_M$  exhibits a characteristic exponential decay with increasing storage time, yielding efficiencies of 10.36% and 1.42% for storage times of  $300\ \mu\text{s}$  and  $1\ \text{ms}$ , respectively. The retrieved echo into the output fiber, thus, contains an estimated mean photon number of  $n_{\text{out}} = n_{\text{in}} \eta_T \eta_M = 14$  and  $n_{\text{out}} = 2$  at  $300\ \mu\text{s}$  and  $1\ \text{ms}$  storage times, respectively. A significant limitation in reducing the mean photon number is the noise from spontaneous emission, which is generated by the CPs acting as imperfect  $\pi$ -pulses. Additionally, the retrieved echo exhibits a broadened Gaussian profile caused by laser wavelength instability, which can be mitigated by stabilizing the laser through cavity locking. More details on characterization of the noise and pulse broadening are discussed in Supplemental Material [53].

*Multimode Capacity*—The practicality of the QM can be significantly improved by storage of modes in different degrees of freedom, as discussed previously. In this section, we showcase the multimode capacity of our QM in temporal as well as spectral degrees of freedom simultaneously. Firstly, we demonstrate storage of a train of 25 temporal modes for a duration of  $800\ \mu\text{s}$  as shown in Fig. 3A. The FWHM of each mode is  $0.75\ \mu\text{s}$  temporally separated by  $7\ \mu\text{s}$  from each other. The maximum number of temporal modes, with a defined memory bandwidth, is mainly constrained by the duration  $\tau_2$  as all the stored modes need to be recalled before the echo of the CP happening after  $\tau_2$  from the second CP (see Fig. S3 in the Supplemental Material).

Next, we demonstrate storage and recall of three spectral modes, each stored in distinct spectral regions of the inhomogeneous broadening and serving as independent memory cells. We first characterize the system and measure negligible crosstalk between adjacent cells separated by 4 MHz when storing a  $0.75\ \mu\text{s}$  wide Lorentzian input pulse [53]. To demonstrate spectro-temporal multi-

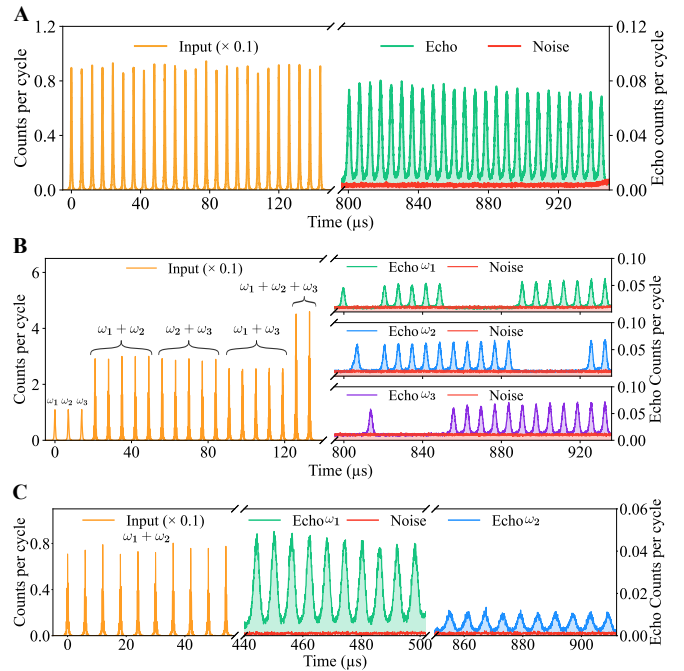


FIG. 3. Demonstration of spectral-temporal multimode capacity. (A) A total of 25 temporal modes, with a defined memory bandwidth, are stored for  $800\ \mu\text{s}$  and subsequently retrieved with an average efficiency of 2.67% and SNR of 9.18. (B) Spectral-temporal multimode capacity with selective recall. The left panel shows a train of 20 temporal modes, where each mode constitutes a various combination of 3 distinct spectral modes ( $\omega_1$ ,  $\omega_2$ , and  $\omega_3$ ) as depicted in the left panel. All prepared modes are stored simultaneously for  $800\ \mu\text{s}$ , while either of the spectral modes is selectively recalled as shown in the right panels. The storage efficiency of the three spectral modes is 1.20%, 1.64%, and 1.66%, respectively. (C) Sequential recall of two spectral modes. The left panel shows a 10 weak coherent pulse input sequence prepared with two spectral modes ( $\omega_1$  and  $\omega_2$ ). After simultaneous storage, they are recalled independently in the same cycle where  $\omega_1$  is retrieved at  $450\ \mu\text{s}$  and  $\omega_2$  is retrieved at  $850\ \mu\text{s}$  yielding efficiencies of 9.33 % and 2.08 %, respectively.

mode operation, we prepare a train of 20 temporal modes with various combinations of three spectral modes at frequencies  $\omega_1$ ,  $\omega_2$ , and  $\omega_3$ , as shown in the left panel of Fig. 3B. The detuning between each spectral mode is set to be 4 MHz for negligible crosstalk. This scenario is analogous to that of probabilistic entangled photon-pair sources, where photon pairs are simultaneously generated over a broad bandwidth [58]. Three consecutive CPs for each spectral mode are applied to enable storage of all the modes. Finally, the selective recall of only the desired spectral mode is performed by applying the corresponding second CP. The recalled output along with the noise for the three spectral modes is shown in the right panels of Fig. 3B. This approach enables simultaneous storage of up to  $20 \times 3 = 60$  modes.

Finally, we demonstrate storage of two spectral modes

and their sequential recall at different storage times, as shown in Fig. 3C. A multi-tone train of 10 input pulses is prepared with frequencies  $\omega_1$  and  $\omega_2$ . Both the spectral modes are stored by applying two simultaneous CPs followed by recall of  $\omega_1$  mode at  $450\ \mu\text{s}$  and recall of  $\omega_2$  mode at  $850\ \mu\text{s}$ . This capability enables the utilization of all the spectral-temporal modes for establishing entanglement across neighboring links in a QR. The spectral multiplexing comes at the cost of the cumulative noise from the spontaneous emission of all active memory cells, as shown by the red noise curve in Fig. 3. Some strategies to mitigate the noise are discussed in the following section.

*Conclusion*—We demonstrate an  $\text{Er}^{3+}$  based telecom QM that integrates the key functionalities required for a practical quantum repeater. The QM supports storage times up to 1 ms with on-demand retrieval, alongside the capability of selective retrieval of multiple spectral modes. In more quantifiable terms, this corresponds to a memory coherence time  $T_2 = 804\ \mu\text{s}$  and initial efficiency  $\eta_o = 23.05\%$ . At the same time, we demonstrated spectral-temporal multimode-capacity with  $3 \times 20$  modes. Though, these parameters do not allow a multiplexed repeater to surpass direct transmission in terms of the probability of entanglement distribution, realistic improvements to  $T_2$  and  $\eta_o$  for the demonstrated degree of multiplexing,  $M = 60$ , would suffice (see Fig. S2A in [53]). Specifically, the  $\eta_o = 65\%$  and  $T_2 = 3\ \text{ms}$  memory parameters generating the curves in Fig. 1, have been achieved experimentally with rare-earth doped YSO.

Towards improving the memory performance, we note that spontaneous decay remains the primary source of noise limiting the signal-to-noise ratio. To bring this down, we may reduce the beam diameter within the crystal to target a smaller ion ensemble, thereby, lowering the amount of emitters. Meanwhile, this would also increase the Rabi-frequency of the CP and, thus, increase the operational bandwidth of the memory while adhering to the adiabaticity condition. To improve the efficiency, and, thus, the output signal strength, we suggest integrating the memory into a critically coupled, low-loss optical cavity. Such a configuration could, in principle, achieve near-unit efficiency [24], although the current state-of-the-art efficiency is approximately 65% [25]. Additionally, the cavity can be engineered to suppress noise and unwanted echoes arising from Purcell-enhanced spontaneous emission [59]. It has also been shown in [40] that the coherence time can be extended to approximately 4 ms by applying a stronger external magnetic field. Combining these improvements in coherence time with cavity enhancements, the proposed memory has the potential to enable quantum repeaters that outperform direct transmission (see supplemental material for detailed calculations [53]).

In conclusion, the proposed improvements provide a clear roadmap to developing QMs that enable a practical

QR and establishes the  $\text{Er}^{3+}:\text{Y}_2\text{SiO}_5$  platform, combined with the CPPE protocol, as a strong candidate for building the hardware required for scalable, long-range quantum networks.

*Acknowledgments*—A.S. would like to thank Alberta Innovates for funding through the Graduate Student Scholarship. This work was supported by the Government of Alberta Major Innovation Fund Project on Quantum Technologies, the National Research Council of Canada through the Small Teams Initiative QPIC, the Department of National Defense through the Innovation for Defence Excellence and Security (IDEaS) program, the Canadian Foundation for Innovation John R. Evans Leaders Fund (CFI-JELF), the Natural Sciences, and the Engineering Research Council of Canada (NSERC) through the Discovery Grant program.

*Author Contribution*—A.S. implemented the experiment and analyzed the data with the help from N.G.K. A.S. and N.G.K drafted the manuscript. D.O. supervised the project. All authors discussed the experimental procedures and results and edited the manuscript.

---

\* Corresponding email: doblak@ucalgary.ca

- [1] H. J. Kimble, *Nature* **453**, 1023 (2008).
- [2] S. Wehner, D. Elkouss, and R. Hanson, *Science* **362**, 10.1126/science.aam9288 (2018).
- [3] D. Cuomo, M. Caleffi, and A. S. Cacciapuoti, *IET Quantum Communication* **1**, 3 (2020).
- [4] V. Giovannetti, L. Maccone, T. Morimae, and T. G. Rudolph, *Physical Review Letters* **111**, 10.1103/physrevlett.111.230501 (2013).
- [5] W. Ge, K. Jacobs, Z. Eldredge, A. V. Gorshkov, and M. Foss-Feig, *Physical Review Letters* **121**, 10.1103/physrevlett.121.043604 (2018).
- [6] T. J. Proctor, P. A. Knott, and J. A. Dunningham, *Physical Review Letters* **120**, 10.1103/physrevlett.120.080501 (2018).
- [7] Z. Zhang and Q. Zhuang, *Quantum Science and Technology* **6**, 043001 (2020).
- [8] P. Kómár, E. M. Kessler, M. Bishof, L. Jiang, A. S. Sørensen, J. Ye, and M. D. Lukin, *Nature Physics* **10**, 582 (2014).
- [9] Q. Zhang, F. Xu, Y.-A. Chen, C.-Z. Peng, and J.-W. Pan, *Optics Express* **26**, 24260 (2018).
- [10] C. Simon, H. De Riedmatten, M. Afzelius, N. Sangouard, H. Zbinden, and N. Gisin, *Physical Review Letters* **98**, 10.1103/physrevlett.98.190503 (2007).
- [11] N. Sangouard, C. Simon, H. De Riedmatten, and N. Gisin, *Reviews of Modern Physics* **83**, 33 (2011).
- [12] A. I. Lvovsky, B. C. Sanders, and W. Tittel, *Nature Photonics* **3**, 706 (2009).
- [13] C. Simon, M. Afzelius, J. Appel, A. B. De La Giroday, S. J. Dewhurst, N. Gisin, C. Y. Hu, F. Jelezko, S. Kröll, J. H. Müller, J. Nunn, E. S. Polzik, J. G. Rarity, H. De Riedmatten, W. Rosenfeld, A. J. Shields, N. Sköld,

R. M. Stevenson, R. Thew, I. A. Walmsley, M. C. Weber, H. Weinfurter, J. Wrachtrup, and R. J. Young, *The European Physical Journal D* **58**, 1 (2010).

[14] S. Wei, B. Jing, X. Zhang, J. Liao, C. Yuan, B. Fan, C. Lyu, D. Zhou, Y. Wang, G. Deng, H. Song, D. Oblak, G. Guo, and Q. Zhou, *Laser & Photonics Review* **16**, 10.1002/lpor.202100219 (2022).

[15] Z. Zhou, C. Liu, C. Li, G. Guo, D. Oblak, M. Lei, A. Faraon, M. Mazzera, and H. De Riedmatten, *Laser & Photonics Review* **17**, 10.1002/lpor.202300257 (2023).

[16] Y. Ma, Y.-Z. Ma, Z.-Q. Zhou, C.-F. Li, and G.-C. Guo, *Nature Communications* **12**, 10.1038/s41467-021-22706-y (2021).

[17] A. Ortú, A. Holzapfel, J. Etesse, and M. Afzelius, *npj Quantum Information* **8**, 10.1038/s41534-022-00541-3 (2022).

[18] F. Wang, M. Ren, W. Sun, M. Guo, M. J. Sellars, R. L. Ahlefeldt, J. G. Bartholomew, J. Yao, S. Liu, and M. Zhong, *PRX Quantum* **6**, 10.1103/prxquantum.6.010302 (2025).

[19] M. Afzelius, C. Simon, H. De Riedmatten, and N. Gisin, *Physical Review A* **79**, 10.1103/physreva.79.052329 (2009).

[20] N. Sinclair, E. Saglamyurek, H. Mallahzadeh, J. A. Slater, M. George, R. Ricken, M. P. Hedges, D. Oblak, C. Simon, W. Sohler, and W. Tittel, *Physical Review Letters* **113**, 10.1103/physrevlett.113.053603 (2014).

[21] P. Jobez, N. Timoney, C. Laplane, J. Etesse, A. Ferrier, P. Goldner, N. Gisin, and M. Afzelius, *Physical review. A/Physical review, A* **93**, 10.1103/physreva.93.032327 (2016).

[22] S.-H. Wei, B. Jing, X.-Y. Zhang, J.-Y. Liao, H. Li, L.-X. You, Z. Wang, Y. Wang, G.-W. Deng, H.-Z. Song, D. Oblak, G.-C. Guo, and Q. Zhou, *npj Quantum Information* **10**, 10.1038/s41534-024-00812-1 (2024).

[23] D. Lago-Rivera, S. Grandi, J. V. Rakonjac, A. Seri, H. De Riedmatten, D. Lago-Rivera, S. Grandi, J. V. Rakonjac, A. Seri, and H. De Riedmatten, *Nature* **594**, 37 (2021).

[24] M. Afzelius and C. Simon, *Physical Review A* **82**, 10.1103/physreva.82.022310 (2010).

[25] S. Duranti, S. Wengerowsky, L. Feldmann, A. Seri, B. Casabone, and H. De Riedmatten, *Optics Express* **32**, 26884 (2024).

[26] J. Jin, E. Saglamyurek, M. L. G. Puigibert, V. Verma, F. Marsili, S. W. Nam, D. Oblak, and W. Tittel, *Physical Review Letters* **115**, 10.1103/physrevlett.115.140501 (2015).

[27] E. Saglamyurek, J. Jin, V. B. Verma, M. D. Shaw, F. Marsili, S. W. Nam, D. Oblak, and W. Tittel, *Nature Photonics* **9**, 83 (2015).

[28] M. L. G. Puigibert, M. F. Askarani, J. H. Davidson, V. B. Verma, M. D. Shaw, S. W. Nam, T. Lutz, G. C. Amaral, D. Oblak, and W. Tittel, *Physical Review Research* **2**, 10.1103/physrevresearch.2.013039 (2020).

[29] N. G. Kamel, A. Mansourzadeh, U. Gautam, V. K. Kavatamane, A. Singh, E. Yeung, D. B. Northeast, P. Barclay, P. J. Poole, D. Dalacu, and D. Oblak, *Erbium-doped fibre quantum memory for chip-integrated quantum-dot single photons at 980 nm* (2025), arXiv:2508.01416 [quant-ph].

[30] M. F. Askarani, M. G. Puigibert, T. Lutz, V. B. Verma, M. D. Shaw, S. W. Nam, N. Sinclair, D. Oblak, and W. Tittel, *Physical Review Applied* **11**, 10.1103/physrevapplied.11.054056 (2019).

[31] X. Zhang, B. Zhang, S. Wei, H. Li, J. Liao, C. Li, G. Deng, Y. Wang, H. Song, L. You, B. Jing, F. Chen, G. Guo, and Q. Zhou, *Science Advances* **9**, 10.1126/sciadv.adf4587 (2023).

[32] M. M. Minnegaliev, K. I. Gerasimov, and S. A. Moiseev, *JETP Letters* **117**, 865 (2023).

[33] M.-H. Jiang, W. Xue, Q. He, Y.-Y. An, X. Zheng, W.-J. Xu, Y.-B. Xie, Y. Lu, S. Zhu, and X.-S. Ma, *Nature Communications* **14**, 10.1038/s41467-023-42741-1 (2023).

[34] S. Yasui, T. Inaba, A. Ishizawa, K. Hitachi, H. Omi, K. Matsuura, R. Kaji, T. Tawara, S. Adachi, X. Xu, and H. Sanada, *Optics Continuum* **3**, 833 (2024).

[35] Z. Li, Y. Lei, T. Kling, and M. Hosseini, *Optica Quantum* **10**, 1364/ opticaq.564321 (2025).

[36] Y.-Y. An, Q. He, W. Xue, M.-H. Jiang, C. Yang, Y.-Q. Lu, S. Zhu, and X.-S. Ma, *Phys. Rev. Lett.* **135**, 010804 (2025).

[37] M. L. Dantec, M. Rančić, S. Lin, E. Billaud, V. Ranjan, D. Flanigan, S. Bertaina, T. Chanelière, P. Goldner, A. Erb, R. B. Liu, D. Estève, D. Vion, E. Flurin, and P. Bertet, *Science Advances* **7**, 10.1126/sciadv.abj9786 (2021).

[38] S. Gupta, R. M. Pettit, A. Sundaresh, V. Niaouris, S. Deckoff-Jones, D. P. Crowley, L. G. Carpenter, A. M. Dibos, M. K. Singh, and S. E. Sullivan, *arXiv* (2025), arXiv:2506.17557 [quant-ph].

[39] Y. Sun, T. Böttger, C. W. Thiel, and R. L. Cone, *Physical Review B - Condensed Matter and Materials Physics* **77**, 10.1103/PhysRevB.77.085124 (2008).

[40] T. Böttger, C. W. Thiel, R. L. Cone, and Y. Sun, *Physical Review B* **79**, 10.1103/physrevb.79.115104 (2009).

[41] J. Dajczgewand, R. Ahlefeldt, T. Böttger, A. Louchet-Chauvet, J. L. Gouët, and T. Chanelière, *New Journal of Physics* **17**, 10.1088/1367-2630/17/2/023031 (2015).

[42] M. Businger, L. Nicolas, T. S. Mejia, A. Ferrier, P. Goldner, and M. Afzelius, *Nature Communications* **13**, 10.1038/s41467-022-33929-y (2022).

[43] T. S. Mejia, L. Nicolas, A. G. Rodriguez, P. Goldner, and M. Afzelius, *arXiv* (2025), arXiv:2507.13973 [quant-ph].

[44] J. S. Stuart, M. Hedges, R. Ahlefeldt, and M. Sellars, *Physical Review Research* **3**, 10.1103/PhysRevResearch.3.L032054 (2021).

[45] M. Rančić, M. P. Hedges, R. L. Ahlefeldt, and M. J. Sellars, *Nature Physics* **14**, 50 (2017).

[46] N. Kukharchyk, D. Sholokhov, A. A. Kalachev, and P. A. Bushev, *Enhancement of optical coherence in 167 ery 2 sio 5 crystal at millikelvin temperatures* (2021).

[47] K. Matsuura, S. Yasui, R. Kaji, H. Sasakura, T. Tawara, and S. Adachi, *arXiv* (2024).

[48] V. Damon, M. Bonarota, A. Louchet-Chauvet, T. Chanelière, and J.-l. L. Gouët, *New Journal of Physics* **13**, 093031 (2011).

[49] F. De Seze, F. Dahes, V. Crozatier, I. Lorgeré, F. Bretenaker, and J.-l. L. Gouët, *The European Physical Journal D* **33**, 343 (2005).

[50] M. F. Pascual-Winter, R.-c. Tongning, T. Chanelière, and J.-l. L. Gouët, *New Journal of Physics* **15**, 055024 (2013).

[51] J. O'Sullivan, O. W. Kennedy, K. Debnath, J. Alexander, C. W. Zollitsch, M. Šiménas, A. Hashim, C. N. Thomas, S. Withington, I. Siddiqi, K. Mølmer, and J. J. L. Morton, *Physical Review X* **12**, 10.1103/physrevx.12.041014 (2022).

- [52] N. G. Kamel, S. Kumar, U. Gautam, E. Saglamyurek, V. Salari, and D. Oblak, [Multimode and random-access optical quantum memory via adiabatic phase imprinting](#) (2025), [arXiv:2506.12223 \[quant-ph\]](#).
- [53] See Supplemental Material at [URL] for additional measurements, and discussion.
- [54] T. Chakraborty, A. Das, H. Van Brug, O. Pietx-Casas, P.-C. Wang, G. C. D. Amaral, A. L. Tchekotareva, and W. Tittel, *npj Quantum Information* **11**, [10.1038/s41534-024-00946-2](#) (2025).
- [55] M. Rancic, M. P. Hedges, R. L. Ahlefeldt, and M. J. Sellars, *Nature Physics* **14**, 50 (2018).
- [56] P. M. Ledingham, W. R. Naylor, J. J. Longdell, S. E. Beavan, and M. J. Sellars, *Physical Review A* **81**, [10.1103/physreva.81.012301](#) (2010).
- [57] C. K. Duda, K. R. Ferguson, R. L. Ahlefeldt, M. P. Hedges, and M. J. Sellars, *Physical review. A/Physical review, A* **107**, [10.1103/physreva.107.1030602](#) (2023).
- [58] Y. Wang, K. D. Jöns, and Z. Sun, *Applied Physics Reviews* **8**, [10.1063/5.0030258](#) (2021).
- [59] X.-X. Li, P. Zhou, Y.-H. Chen, and X. Zhang, *Physical review. A/Physical review, A* **108**, [10.1103/physreva.108.012614](#) (2023).